Solar wind interactions with comet C/2021 A1 Using STEREO HI and a data-assimilative solar wind model

Article

Published Version

It is advisable to refer to the publisher's version if you intend to cite from the work. See Guidance on citing.

www.reading.ac.uk/centaur

CentAUR

Central Archive at the University of Reading

Reading's research outputs online

CrossMark

Solar Wind Interactions with Comet C/2021 A1 Using STEREO HI and a Data-assimilative Solar Wind Model

Sarah R. Watson[ID], Christopher J. Scott[ID], Mathew J. Owens[ID], and Luke A. Barnard[ID]
University of Reading, Whiteknights House, Reading, RG6 6UR, UK; s.r.watson@pgr.reading.ac.uk
Received 2024 February 12; revised 2024 May 20; accepted 2024 May 26; published 2024 July 22

Abstract

Cometary tails display dynamic behavior attributed to interactions with solar wind structures. Consequently, comet-tail observations can serve as in situ solar wind monitors. During 2021 December, Comet Leonard (C/2021 A1) was observed by the STEREO-A heliospheric imager. The comet tail exhibited various signatures of interactions with the solar wind including bending, kink formation, and finally complete disconnection. In this study, we compare the timing of these events with solar wind structures predicted by the Heliospheric Upwind eXtrapolation model with a time-dependency (or HUXt) solar wind model using new solar wind data assimilation (DA) techniques. This serves both to provide the most accurate solar wind context to interpret the cometary processes, but also as a test of the DA and an example of how comet observations can be used in model validation studies. Coronal mass ejections, stream interaction regions (SIRs), and heliospheric current sheet (HCS) crossings were all considered as potential causes of the tail disconnection. The results suggest the tail disconnection at Comet Leonard was the result of it crossing the HCS and into an SIR. The timing of these features agree better with the DA model results than the non-DA model, showing the value of this approach. Case studies such as this expand our understanding of comet–solar wind interactions, and in demonstrating the utility of DA for solar wind modeling. We note that this could lead to comets acting as additional in situ measures for solar wind conditions for regions where no in situ spacecraft are available, potentially improving solar wind DA in the future.

Unified Astronomy Thesaurus concepts: Comets (280); Solar wind (1534); Comet tails (274)

Materials only available in the online version of record: animation

1. Introduction

Comets are influenced by structure in the solar wind through which they are moving, revealing information about both the comets themselves and the local solar wind conditions. A comprehensive review of previous case studies and the potential use of comet-tail observations as proxy solar wind data are discussed in Jones et al. (2018, and references therein). As comets approach the Sun, the increased thermal energy causes their icy composition to sublimate into gas, forming the coma, dust and plasma tails (Götz et al. 2022). A comet has two types of tail: a dust tail, which follows the orbit of the comet (appearing curved), and a plasma tail, which points almost radially away from the Sun and is shaped by the solar wind (Voelzke 2005). The plasma tail can interact with the solar wind in different ways, with some interactions resulting in a complete removal of a section of the tail, known as a disconnection event.

There is a range of techniques to investigate disconnection events. Many use modeling techniques to give an indication of the solar wind conditions at the desired location and compare these to observations. For example, Wegmann (2000) used magnetohydrodynamic (MHD) models to describe the effects of different solar wind disturbances on cometary tails, whereas Jia et al. (2007, 2009) used MHD simulations to reproduce the conditions needed for a disconnection and compared these to observations at STEREO-A. Methods have also been developed to use comet observations to determine the local

solar wind conditions. Ramanjooloo & Jones (2022) demonstrated a novel technique to obtain solar wind velocities from a single image of a comet, whereas Price et al. (2019) used a temporal-mapping technique applied to comet dust tails to determine how they are influenced by the solar wind. The latter technique also allowed images from different sources to be compared, which some techniques do not allow. These methods allow us to better understand these disconnection events and the associated solar wind dynamics.

To add to the tools available for comet-tail interpretation, this paper describes a novel approach of adding data assimilation (DA) to a reduced-physics model of the solar wind in order to obtain the most accurate reconstruction of the local conditions at the comet. DA is used to improve the model output in meteorology, both to improve forecasting and as "reanalysis," to retrospectively provide the best global reconstruction of the atmosphere, combining models and observations (e.g., Kalnay 2002; Migliorini & Candy 2019). This approach is used in some solar and coronal science, and is now starting to be adopted in heliospheric science too (Owens et al. 2019). We here show how it can improve and allow for a more accurate analysis of the solar wind conditions at the location of the comet. This will also act as a test for the model performance. Individual studies such as the one described here are key to improving our understanding of comet-tail disconnections as they can bridge the gap between theory and observations and provide specific examples for comparison with models.

In Section 2, we review types of solar wind structures and their interactions with comets, as well as discuss previous case studies. In Section 3, we introduce Comet Leonard (C/2021 A1) and the observations used within this case study. In

Section 4, we outline the methods used to analyze this disconnection event, mainly the Heliospheric Upwind eXtrapolation model with time-dependency (HUXt) solar wind model and DA techniques. In Section 5, we combine the observations and data assimilative solar wind model to discuss the cause of the disconnection event. In Section 6, the results are summarized and discussed.

2. Solar Wind Structures and Their Interactions with Comets

A comet plasma tail is directly influenced by the properties of the local solar wind. Comet tails are observed to undergo multiple disconnection events, for example comet 1P/Halley in 1986 April, where two disconnection events were observed (Lundstedt & Magnusson 1987). Disconnection events have been explained by the passage of a heliospheric current sheet (HCS, a boundary separating positive and negative magnetic field) crossing (e.g., Brandt et al. 1999; Kuchar et al. 2008), a stream interaction region (SIR, a region of fast solar wind interacting with the preceding slow solar wind; Wegmann 2000), or a coronal mass ejection (CME, a sudden outburst of magnetic flux and energetic particles from the surface of the Sun; e.g., Vourlidas et al. 2008; Jia et al. 2009).

2.1. Heliospheric Current Sheet

The solar wind flows radially outwards from the Sun and drags the coronal magnetic field with it due to the frozen-in flux theorem (Alfvén 1942). The rotation of the Sun causes this to be wound into a spiral shape, known as the Parker spiral (Parker 1958), which extends through the solar system. The HCS is the boundary between the heliospheric magnetic field that points toward and away from the Sun. There have been many studies on the link between HCS crossings and comet-tail disconnection events (e.g., Niedner & Brandt 1978; Yi 1994; Brandt et al. 1999; Voelzke & Matsuura 2000), with some of these studies suggesting a crossing of the HCS was the primary cause of disconnection events in comets (e.g., Yi 1994). However, other studies suggest it is not a necessary condition for a disconnection event, with other mechanisms at play (Delva et al. 1991). Further to this, in research by Brosius et al. (1987) on the disconnection event in Comet 1P/Halley, it was found that there is a time delay between the crossing of the HCS and the disconnection of the tail. It was assumed to be in the range of 0.1–0.6 days (Brosius et al. 1987). This delay in the crossing of the HCS and the disconnection suggests that another solar wind structure which occurs in conjunction with HCS crossings could actually be the trigger of these disconnections. As the HCS is often embedded within an SIR, a fast solar wind stream is a likely candidate (Wegmann 2000).

2.2. Stream Interaction Regions

The solar wind can be broadly categorized into a slow ($\sim$400 km s^{-1}) and a fast wind ($\sim$750 km s^{-1}). These classes differ not only by their speed, but also by their density, ion composition, and coronal origin (Ebert et al. 2009). Slow solar wind tends to originate from closed magnetic field lines associated with the streamer belt, whereas fast solar wind originates from open magnetic field lines within coronal holes (e.g., Owens 2020, and references therein). The variation of the fast and slow solar wind in the heliosphere, combined with the

rotation of the Sun, results in SIRs. Specifically, the fast solar wind catches up with the slower wind ahead, causing an interaction region where the slow wind is accelerated and the fast wind is decelerated, forming a region of compressed plasma (Allen et al. 2021). Since the HCS is typically surrounded by slow solar wind, as it originates from the streamer belt (Antiochos et al. 2011), the HCS is typically bound within the SIR. Thomas et al. (2014) used a superposed epoch analysis of HCS crossings to show the relationship between the solar wind speed and the magnetic field polarity around the time of HCS crossings. They showed that an HCS crossing is often accompanied with a transition from a slow stream to a fast stream. However, not all slow solar winds are associated with the HCS, and not all HCS crossings are associated with SIRs. Jian et al. (2019) analyzed SIR events observed by STEREO-A and reported that only 54% of the SIR events were associated with an HCS, and therefore an SIR should be considered as its own mechanism for comet-tail disconnection events.

2.3. Coronal Mass Ejection

Furthermore, there have been observations of a third mechanism: an interaction with a CME. CME-induced comet-tail disconnections have been observed by the STEREO spacecraft before (e.g., Kuchar et al. 2008; Vourlidas et al. 2008; Jia et al. 2009). Prior to the STEREO mission, observations of CME-driven comet disconnections were rare, but the introduction of STEREO's two Heliospheric Imagers (H-1 and H-2) allowed CMEs and comets to be observed in the same field of view, making these interactions easier to detect. However, there are still some reports of CME-induced interactions prior to STEREO. In a paper by Jones & Brandt (2004), three comet-tail disturbances of comet 153/Ikeya-Zhang were investigated, with each interaction being associated with a CME passage. They suggested that these interactions could be used to identify fast CME locations within the heliosphere (Jones & Brandt 2004). In addition to these remote observations, there have also been in situ observations of CME–comet interactions. Comet 67P was visited by Rosetta, during which time in situ observations were made of a CME that directly influenced the plasma environment of the comet (Edberg et al. 2016). These studies highlight the importance of also investigating CMEs as a potential cause of comet disconnection events.

3. Observations

Comet Leonard (C/2021 A1) is a long-period comet that was first observed in 2021 January by G. J. Leonard. It reached perihelion (0.615 au) on 2022 January 3 and passed by Venus at close proximity (0.029 au) on 2021 December 18 (Zhang et al. 2021). This study investigates the tail disconnection event of Comet Leonard, which occurred in 2021 December and was observed by the STEREO-A spacecraft (Kaiser et al. 2008). The STEREO spacecraft have observed disconnection events before, such as when a CME caused the disconnection of Comet Encke (Vourlidas et al. 2008). The fact that the Leonard disconnection event occurred close to the ecliptic plane enables us to use a new method for interpretation of the observations. The HUXt solar wind model (described below), initialized with solar wind speeds generated by combining the output of a coronal model and
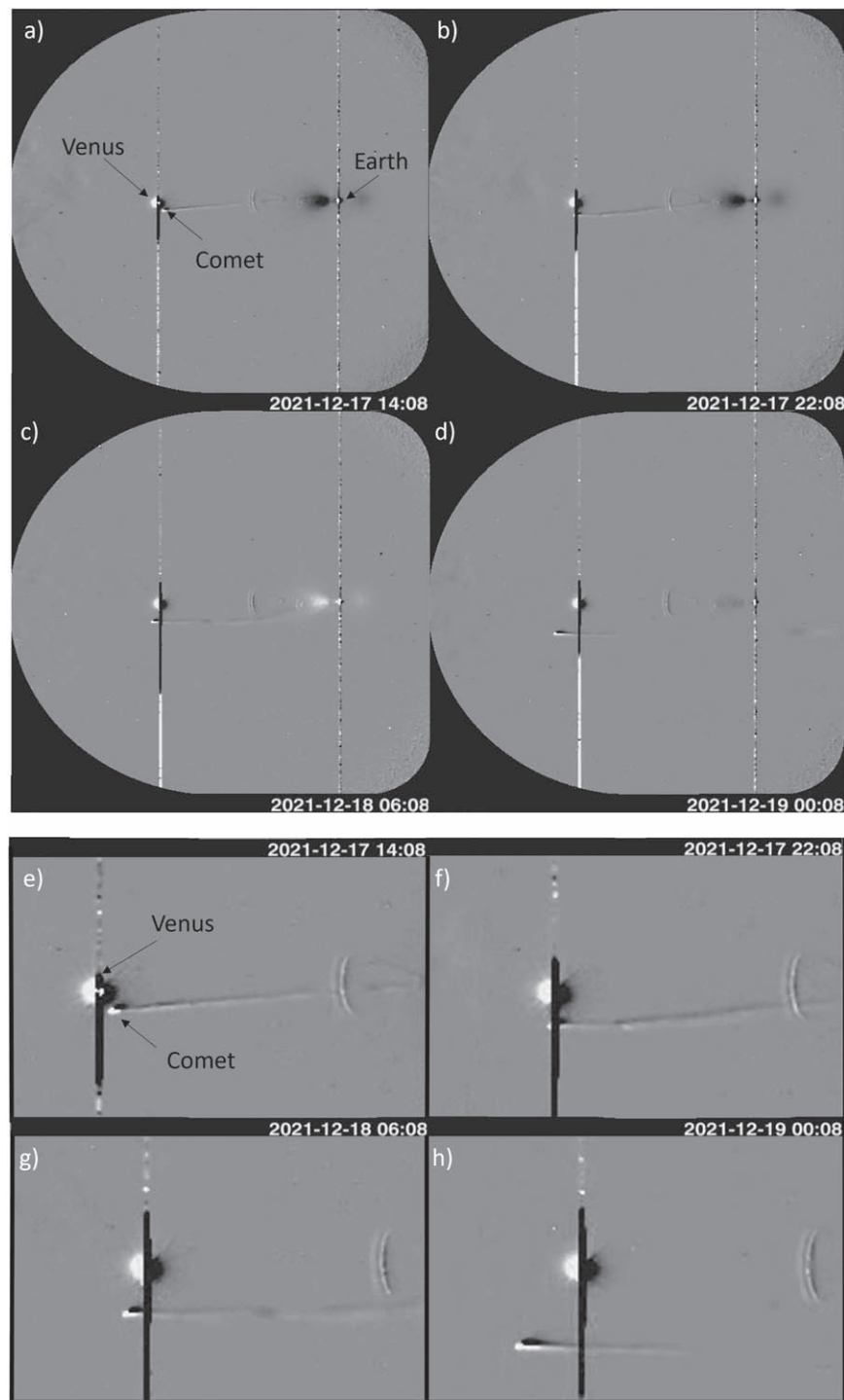
Figure 1. The disconnection event of Comet Leonard observed by the STEREO-A HI-2 camera. These images ((a)–(h)) are snapshots from the difference movies, provided by RAL Space, over a time period of 34 hr which best highlights the event. The Sun is off to the left, out of view of the camera. The bright object on the left is the planet Venus, and the one on the right is Earth (both labeled in panel (a)). Image (a) depicts the comet before the disconnection as it approaches Venus, with its tail extending outwards behind the nucleus. Image (b) shows a small kink forming at about a quarter of the way down the length of the tail. Image (c) shows the disconnection of the tail with a visible gap between the two sections, and image (d) shows the comet shortly after the disconnection, with a visibly shorter tail. Images (e), (f), (g), and (h) are the same time stamps as (a), (b), (c), and (d), respectively, but zoomed in. The full movie is available as an animation. In the animation, the comet appears as a small dot in the top center around 2 s in (timestamp 2021 December 6 00:08). The tail then becomes more visible, with the disconnection event occurring 6 s in (timestamp 2021 December 17 14:08, to 2021 December 19 00:08). The animation does not include the annotations of the planets or comet and runs for a longer period (timestamp 2021 December 1 02:09 to 2021 December 31 22:08). The animation also does not include the zoomed-in version.

(An animation of this figure is available in the online article.)

in situ data measured by spacecraft at 1 au, provides an optimum estimate of the ambient solar wind conditions in the inner heliosphere. As in situ observations are currently limited to the ecliptic plane, the solar wind can be most accurately reconstructed close to the solar equator. This enabled a simple and reliable comparison between the STEREO-A observations and the colocated solar wind at the time of the tail disconnection.
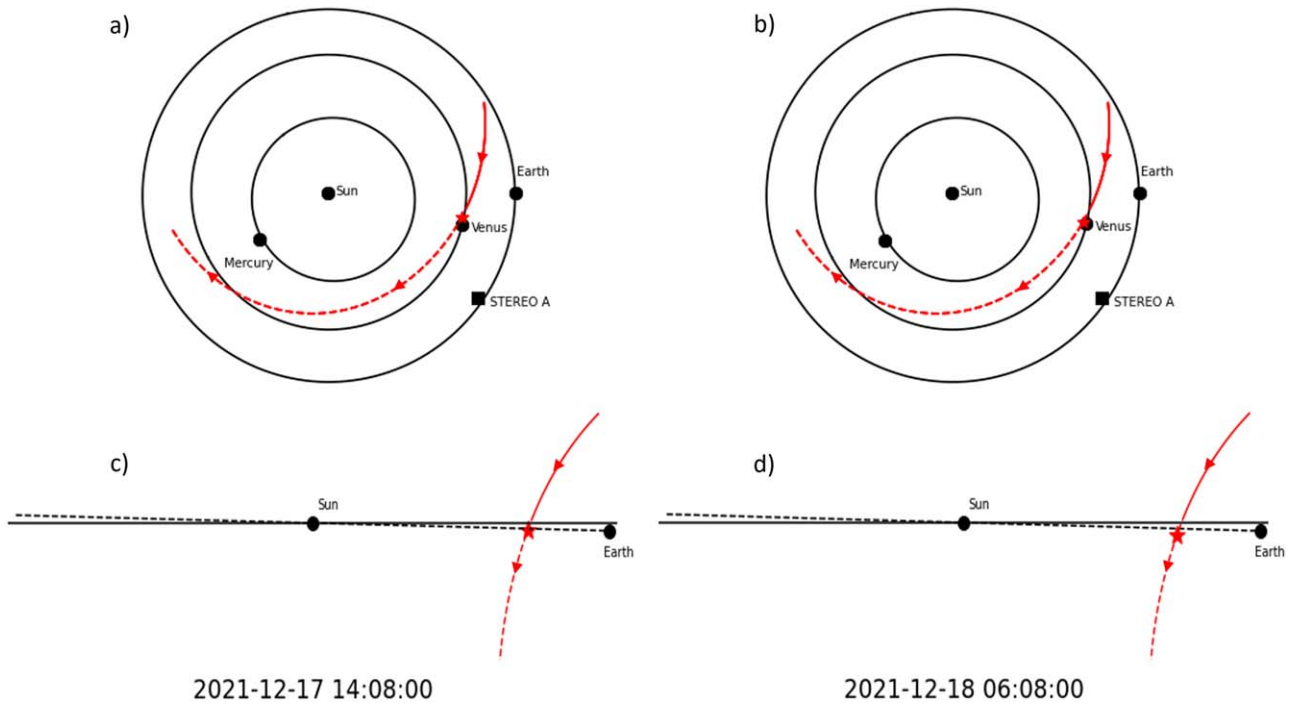
Figure 2. The position of Comet Leonard for the interval 2021 December 17 14:08 UTC to 2021 December 18 06:08 UTC along with the position of the inner planets and STEREO-A. The trajectory of Comet Leonard is shown in red and the direction indicated by the arrows. The solid red line represents the trajectory above the ecliptic and the dashed red line represents the trajectory below the ecliptic. The red star indicates the position of Comet Leonard at the given time. The top row ((a) and (b)) is the view from the north ecliptic plane. The bottom row ((c) and (d)) shows the comet with respect to the solar equatorial plane (solid line) and the Earth ecliptic plane (dashed line).

3.1. Comet Leonard in the HI-2 Camera

The Heliospheric Imager-2 (HI-2) camera is part of the Sun-Earth Connection Coronal and Heliospheric Investigation (or SECCHI) instrument package on board the STEREO-A spacecraft (Howard et al. 2008). The HI-2 camera has a circular field of view with a diameter of 70° and an image cadence of 2 hr (Eyles et al. 2009). It captured images of Comet Leonard during 2021 December. Figure 1 shows Comet Leonard in the field of view of the STEREO HI-2 camera over a period of 72 hr from 2021 December 16 to 19 (see animation). This is a difference movie, which highlights differences in consecutive frames, with the differences between the frames appearing as light/dark patches, allowing for moving objects to be seen clearly.[1] Difference images are used in this paper to highlight the comet-tail disconnection clearly as these types of images emphasize this event, especially the disconnection point. However, for the calculations and extracting of information such as speed and timings, we use nondifference images. The images shown (Figures 1(a)–(h)) are frames extracted from these difference movies. The comet first becomes visible in the HI-2A camera on 2021 December 3, with the disconnection event occurring on December 18. The top panels of Figures 1(a)–(d) show a time sequence of four images which best capture the disconnection event. The bottom panels, labeled Figures 1(e)–(h), show the same four times, but zoomed in to show the details of the comet tail. Figure 1(e) depicts the comet before the disconnection as it approaches Venus, with its tail extending outwards behind the nucleus. The next image, Figure 1(f), shows a small kink forming at about a

quarter of the way down the length of the tail. Figure 1(g) shows the disconnection of the tail with a visible gap between the two sections, and Figure 1(h) shows the comet shortly after the disconnection, with a visibly shorter tail. The disconnected tail is swept away antisunwards, to the right of the images. Based on these images, the disconnection event can be summarized as the following sequence of events:

1. 2021 December 17 14:08 UTC: tail starts to deform upwards.
2. 2021 December 17 14:08 UTC to 2021 December 18 06:08 UTC: kink travels down the tail.
3. 2021 December 18 06:08 UTC: tail is totally removed.

The remainder of this paper will therefore focus on the interval 2021 December 17 14:08 UTC to 2021 December 18 06:08 UTC as the time interval during which a change in the solar wind conditions at the comet is suggested.

3.2. Ephemeris of Comet Leonard

Comet Leonard's position was obtained using the JPL Horizons database for the period being investigated.[2] Its position relative to the Sun, the inner planets, and STEREO-A is shown in Figure 2, both in the ecliptic (top) and perpendicular to the ecliptic (bottom). This shows that Comet Leonard's latitude remained close to the ecliptic plane throughout the period of interest. While the model used to investigate the solar wind can reconstruct conditions at all solar latitudes, DA of measurements from in situ spacecraft (discussed later) is most effective in this plane as it is where these measurements were made (in this case, from STEREO-A

---

[1] See "The Heliospheric Imager for the NASA STEREO Mission," available online: http://www.stereo.rl.ac.uk.

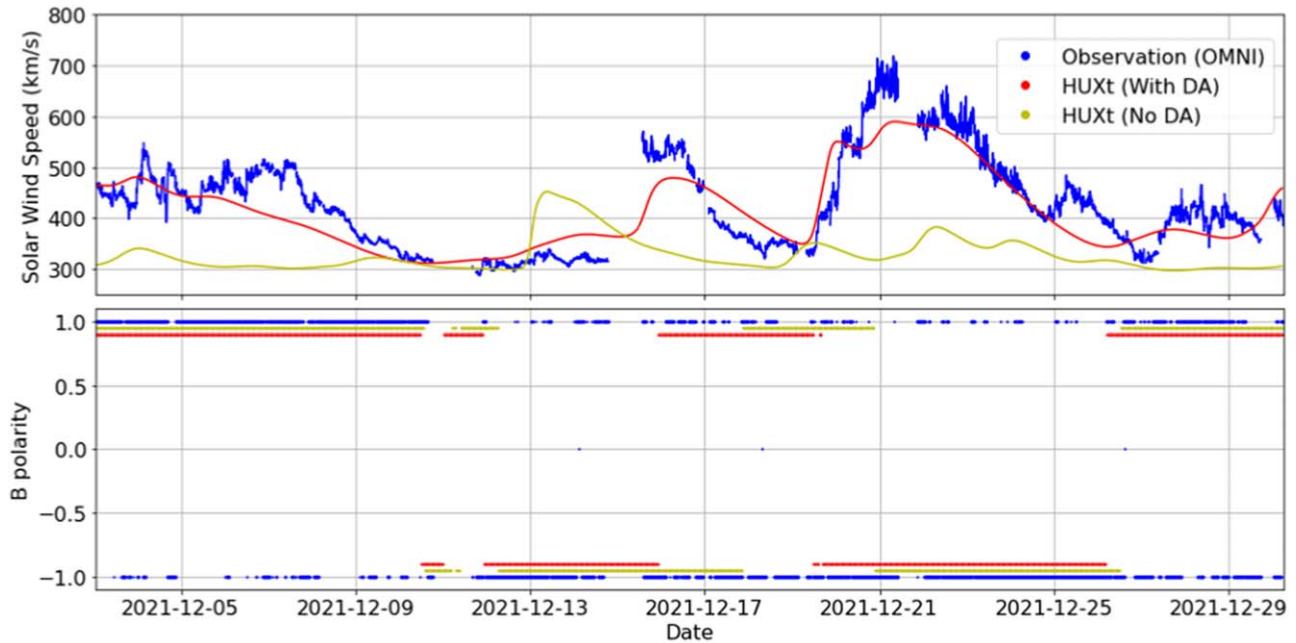[2] http://ssd.jpl.nasa.gov/horizons/app.html

Figure 3. A time series of the solar wind speed (top) and magnetic field polarity (bottom) at L1 for 2021 December. The MAS/HUXt model run (No Data-Assimilation) is shown in yellow and the MAS/BRaVDA/HUXt model run (Data-Assimilation) is shown in red, along with the observational data obtained from OMNI shown in blue over the same time period.

and the Advanced Composition Explorer, ACE, spacecraft). The fact that the comet was passing through the solar equatorial plane as the disconnection event occurred means it serves as the ideal case study to test this new technique.

4. Methods

4.1. HUXt Model

Solar wind structures and their three-dimensional positions are hard to identify within the HI images alone. Here, the disconnection event is investigated using the Heliospheric Upwind eXtrapolation model with time-dependency (HUXt) model (Owens et al. 2020; Barnard & Owens 2022). HUXt is a reduced-physics model of the solar wind. It uses approximations to simplify the three-dimensional MHD equations to one-dimensional hydrodynamic physics, but still gives a comparable solar wind structure (Riley & Lionello 2011). This makes it faster and simpler to run than MHD, making it suitable for using with DA. It can accurately propagate and evolve solar wind conditions from a near-Sun inner boundary (typically 0.1 au) through the inner heliosphere. The solar wind at the HUXt inner boundary is typically determined by the output of magnetogram-constrained coronal models, such as the Wang–Sheeley–Arge (or WSA; Arge & Pizzo 2000), magnetohydrodynamics-about-a-sphere (MAS; Riley et al. 2001), or the Durham magnetofrictional (or DUMFRIC; Yeates et al. 2010) models. For this study, the MAS coronal model was used, which simulates coronal conditions at 30 $R_\odot$ to determine the solar wind speed. Data are available online.[3]

As well as solar wind speed, HUXt can also estimate the magnetic polarity and location of the HCS throughout the heliosphere. HUXt does this by computing streaklines of the flow and using these to map outwards the magnetic polarity at the inner boundary condition, assuming that the magnetic field

advects passively with the solar wind flow (Barnard & Owens 2022).

The HUXt results for near-Earth space are shown in Figure 3 along with the observations obtained from OMNI. The HUXt/ MAS results do not agree with the OMNI (observations) data on the positions of certain structures, and the model appears to underestimate the solar wind speed routinely throughout the selected period.

4.2. Data Assimilation

Data assimilation (DA) combines observations and models to produce an improved estimate of the global state of a system. It has recently been applied to in situ observations of the solar wind (Lang et al. 2021). In the current study, the STEREO-A and ACE spacecraft were the only suitable in situ observations available at the time of the disconnection event. The Burger Radial Variational Data Assimilation (BRaVDA) solar wind scheme was used to assimilate the data from these two spacecraft (STEREO-A and ACE) into the solar wind model. A full description of the BRaVDA methodology can be found in Lang & Owens (2019). The MAS coronal model for the Carrington rotation being investigated (CR 2252) provided the prior state of the solar wind conditions in the DA analysis. The minimum cost function between the prior and in situ observations is calculated by BRaVDA, and the inner boundary conditions are then produced. These inner boundary conditions were then used to initialize HUXt to give a more accurate representation of the solar wind conditions at the location of Comet Leonard. Before comparing with the STEREO/HI observations, it is instructive to examine the model results in near-Earth space. Figure 3 shows that the DA run of HUXt (in red) more accurately represents the solar wind conditions observed (OMNI data shown in blue) during this time than the non-DA HUXt run (in yellow). The features of the solar wind (such as prominent fast streams and magnetic field polarity changes) measured by near-Earth in situ observations are well

---

[3] https://www.predsci.com/data/runs/cr2252-high/hmi_mast_mas_std_0101/helio/

Figure 4. A time series of the solar wind speed (top) and magnetic field polarity (bottom) at STEREO-A for 2021 December. The MAS/HUXt model run (No Data-Assimilation) is shown in yellow and the MAS/BRaVDA/HUXt model run (Data-Assimilation) is shown in red, along with the observational data obtained from STEREO-A shown in blue over the same time period.

portrayed by the DA run of the HUXt model. This highlights the importance of the use of DA in models in order to accurately portray the solar wind conditions at a given location. However, from the comparison to OMNI alone, it is hard to determine how well the model performs at other locations in the solar system. Therefore, the model output was also examined at the location of STEREO-A (see Figure 4). During the time period of the model run, the STEREO-A spacecraft was located at a longitudinal separation angle of approximately 35° with Earth and therefore experienced different solar wind structures at different times to that of Earth. Figure 4 shows again that the DA run of HUXt (red) more accurately represents the solar wind conditions measured by the STEREO-A spacecraft (blue) than the non-DA HUXt run (yellow). The conformity of the model with two individual observational data sets located at solar longitudes either side of the comet gives a strong indication that the model will accurately represent the solar wind conditions at the location of Comet Leonard. In the following section, we test this by using the observations of Comet Leonard and comparing them to the model output.

5. Results

Following the review of previous tail disconnection events in Section 2, the three potential solar wind structures were investigated using the HUXt model to determine the cause of this tail disconnection, and to determine if the agreement in the timing of the simulated solar wind structures and observed comet-tail events is improved by DA.

5.1. Coronal Mass Ejection

The online catalog provides a list of parameters from CMEs observed by the Solar and Heliospheric Observatory's Large Angle and Spectromeric Coronagraph Experiment instrument.[4]

There were a number of CMEs around the time of the disconnection, but from these parameters alone it is hard to determine if they were directed at the comet. From Figure 2, it is clear that the comet was close to the Earth–Sun line, and therefore it is reasonable to assume a CME that impacted Earth during this period will also have interacted with Comet Leonard. Using the "Near-Earth Interplanetary Coronal Mass Ejections Since 1996 January" catalog, it was determined that there were no CME impacts with Earth at the time of the comet disconnection, and therefore it can be assumed there was no CME impact at the comet. Thus, a CME was ruled out as a cause for the disconnection event.[5]

5.2. Heliospheric Current Sheet Crossing

Figure 5 shows the results of without DA, i.e., the MAS/HUXt model (left: plots (a)–(d)), as well as with DA, i.e., the MAS/BRaVDA/HUXt model (right: plots (e)–(h)) for comparison, for the two times of interest. Without DA, the model indicates the HCS has not reached Comet Leonard at the time the disconnection event starts (at 2021 December 17 14:08 UTC; Figure 5(a)). At the second epoch (2021 December 18 06:00 UTC), the model shows that Comet Leonard has just crossed from a positive-polarity sector (purple) into a negative-polarity sector (orange; Figure 5(c)), signifying the HCS location. This would suggest that the initial kink forming in the tail at 2021 December 17 14:08 UTC, was not as a result of the HCS, but that the complete removal of the tail at 2021 December 18 06:00 UTC could be. However, this does not support the observations by Brosius et al. (1987), discussed in Section 2.1, which suggested a delay of 0.1–0.6 days between crossing the HCS and the disconnection. This also ignores the clear distortion of the comet tail seen by STEREO prior to this crossing, and does not provide a plausible cause for this. Therefore, we consider that the non-DA (MAS/HUXt)
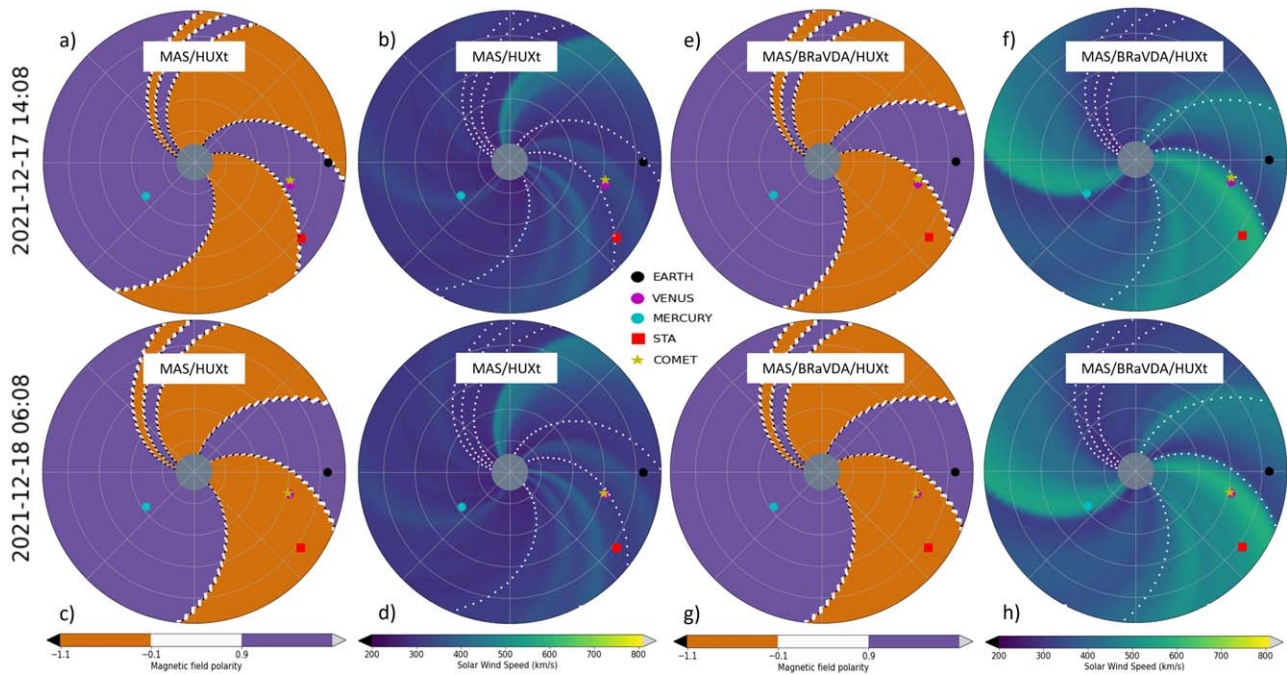

Figure 5. Results from the MAS/HUXt model (left: plots (a)–(d)) and the data assimilative MAS/BRaVDA/HUXt model (right: plots (e)–(h)). Plots (a) and (e) show the position of the HCS for the epoch 2021 December 17 14:08 UTC, and plots (c) and (g) show the position of the HCS at 2021 December 18 06:08 UTC. The purple regions indicate positive magnetic field polarity and the orange indicate negative polarity, with the white lines indicating the position of the HCS. Plots (b) and (f) show the solar wind speed at the epoch 2021 December 17 14:08 UTC, and plots (d) and (h) show the solar wind speed at 2021 December 18 06:08 UTC. The regions of darker blue represent slower solar wind and the lighter regions show regions of faster solar wind. The position of Comet Leonard is shown by the yellow star and the positions of the STEREO-A spacecraft, Earth, and the two inner planets are also shown.

simulation fails to provide a plausible explanation for the sequence of events at Comet Leonard observed by STEREO HI-2. Next, the observations were compared to the DA (MAS/BRaVDA/HUXt) model to determine whether the addition of DA better represents the observations seen by STEREO. Figure 5(e) shows the position of Comet Leonard to be at the location of the HCS at the first epoch (2021 December 17 14:08 UTC) and therefore coincides with the start of the kink forming in the tail. Figure 5(g) shows the comet well past the HCS at the time the tail is fully disconnected (2021 December 18 06:00 UTC), which supports the theory proposed by Brosius et al. (1987), suggesting the disconnection occurs some time after the crossing. This highlights the possibility of there being another structure involved in this disconnection event.

5.3. Stream Interaction Region

The possibility of an SIR as a candidate for the disconnection event was investigated. The same method was used. Figures 5(b) and (d) show no significant change in the solar wind speed at the location of Comet Leonard in either epoch, indicating this could not be the mechanism for the disconnection. This is not supported by the observations seen by the STEREO HI-2 camera, where Comet Leonard experiences solar wind interactions, beginning at 2021 December 17 14:08 UTC. However, when using DA (MAS/BRaVDA/HUXt), Figures 5(f) and (h) show a potential SIR around the location of the comet at the time of interest. This is shown by the transition between slower solar wind (darker blue) to faster solar wind (lighter blue). MAS/BRaVDA/HUXt also suggests that this SIR is associated with the HCS, seen as the white dotted line on the plot. Previous studies suggest that the bending of the tail seen in the STEREO images

can indicate the comet passing from a region of slow wind to fast wind (Wegmann 2000). Without DA, this model argues against an SIR as a mechanism for the disconnection event observed, due to the absence of any fast wind near the comet at the time. The DA model, however, supports the theory that the delay in the disconnection after crossing the HCS is due to an SIR that follows, and therefore better aligns with other observations of disconnection events mentioned in Section 2.1. This further supports the need for DA in improving the accuracy of the model to ensure it can accurately explain observations seen in the STEREO HI-2 images.

5.4. Solar Wind Conditions at Comet Leonard

A time series of the solar wind conditions at Comet Leonard is shown in Figure 6. Again, the clear differences between the no-DA (MAS/HUXt: black) and the DA (MAS/BRaVDA/HUXt: red) model solar wind conditions are apparent. This is more prominent in Figure 6(b), where the DA solar wind speed increases during the time the kink is seen in STEREO, whereas the non-DA remains at a constant speed. Additionally, the DA-modeled HCS crossing time at Comet Leonard better matches the HI observations, occurring at the time the kink is seen to begin forming in the STEREO images (blue vertical line in plot (b)). The DA highlights that the change in polarity is followed by an increase in speed. The non-DA does not show this, and therefore it could have been interpreted that the disconnection was due to the HCS crossing alone and not one followed by an SIR.

To further compare the HUXt model to the STEREO observations, the solar wind speed was inferred by assuming the tail disconnection is carried away from the comet nucleus at the local solar wind speed. For this calculation, the original
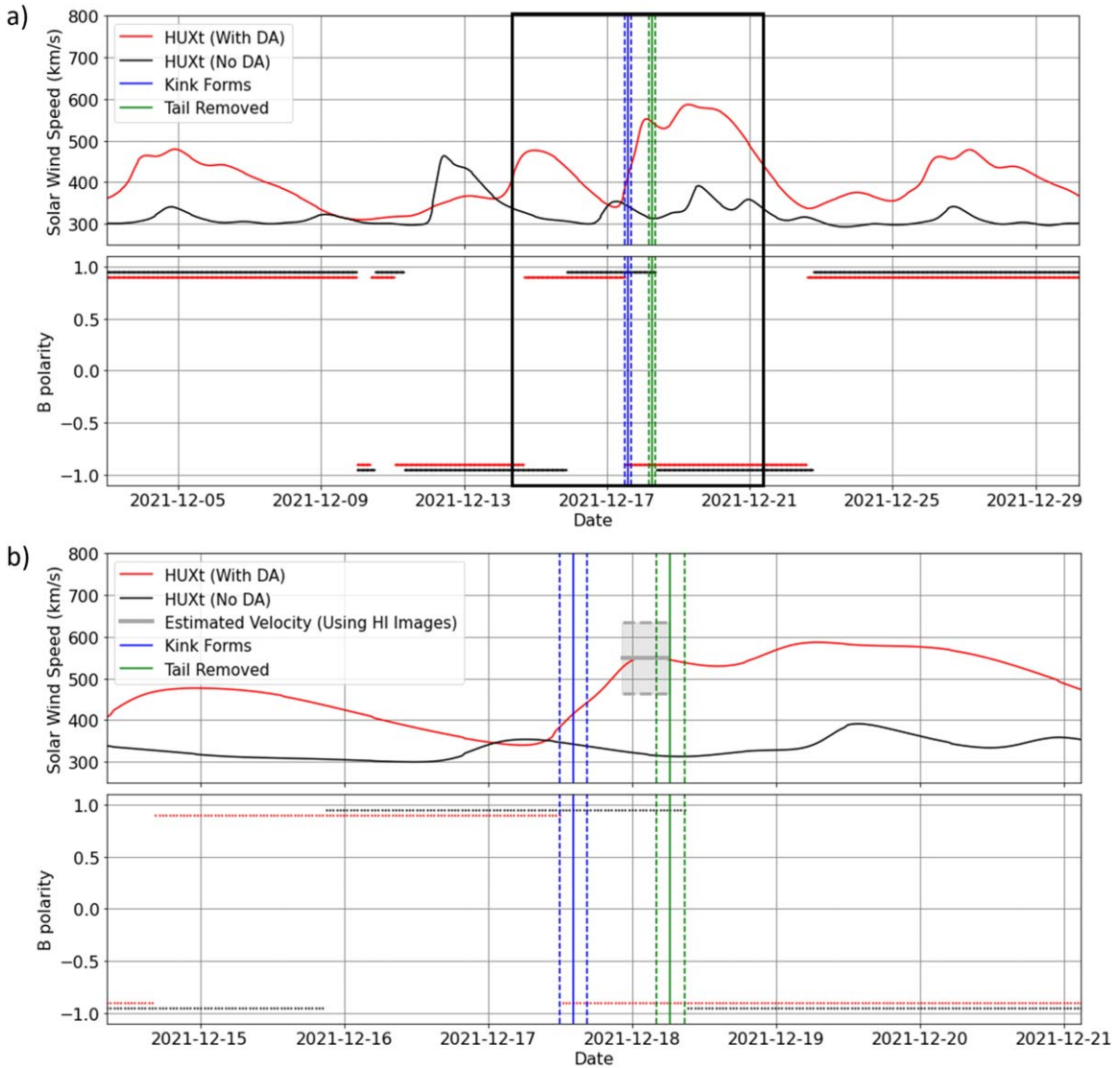
Figure 6. The top panel (a) shows the solar wind speed and magnetic field polarity at the location of Comet Leonard for 2021 December. The MAS/HUXt model run (No Data-Assimilation) is shown in black and the MAS/BRaVDA/HUXt model (Data-Assimilation) is shown in red. The times at which the kink forms and the total removal of the tail occurs have been marked by the blue and green lines, respectively, along with their associated error bars (obtained from the image cadence), represented by the dashed lines. The bottom panel (b) shows the same plot, but focused on the time period of interest outlined by the black area in the top panel. The gray solid line indicates the estimated solar wind speed calculated from the HI images, along with the associated errors marked by the gray dashed lines. The horizontal extent of the shaded area indicates the time period of the HI images that were used to calculate the velocity.

STEREO images were used (not the difference images shown in Figure 1) to infer the position of the tail disconnection during two times (indicated by the horizontal extent of the gray shaded area in Figure 6). Assuming the comet was traveling at a constant speed during this time period, and that the comet tail was entirely radial from the Sun, the speed of the comet-tail disconnection was calculated from the HI images to be $549 \pm 86 \, \mathrm{km \, s^{-1}}$ (gray solid line on Figure 6(b)). Although this calculated speed is an average of the speed between two times, it does indicate that the local solar wind conditions were representative of that of a fast solar wind stream and shows a strong agreement with the DA run. As mentioned previously, the DA run of the HUXt model shows an increase in solar wind speed after the initial crossing of the current sheet (Figure 6), whereas the non-DA run shows the solar wind speed close to ambient and therefore does not reflect the observations. This further highlights the improved correlation between the HUXt model output and the observations after the addition of DA.

6. Discussion

Using HI observations of Comet Leonard and solar wind modeling, this study has investigated a comet-tail disconnection being a result of the comet crossing the HCS and into an SIR. Combining the observations with the MAS/HUXt model without the use of in situ DA gave an implausible result for the cause of the disconnection. In particular, there was no modeled solar wind structure at the time of the tail kink formation. It did, however, indicate that there may have been an HCS crossing close to the end of the time of interest (2021 December 18 06:00 UTC). However, this was further complicated by the disconnection delay seen after crossing the HCS observed in other literature (Niedner & Brandt 1979; Brosius et al. 1987), which would suggest that the HCS shown in the model occurred too late when compared with observations and therefore would have been ruled out as the cause. The lack of obvious agreement between the modeled solar wind

structure and the comet observations can be interpreted as the model not correctly reproducing the solar wind structure at that location.

Adding DA to the model (MAS/BRaVDA/HUXt) significantly improved the correspondence between the model solar wind structure and timing of comet-tail activity. This can be summarized as follows:

1. The model shows the comet crossing the HCS at 2021 December 17 10:00 UTC. The STEREO HI images then show a kink in the comet tail form shortly after this time at 2021 December 17, 14:08.
2. At the same time as the HCS crossing, the model shows the comet entering into an SIR. The STEREO HI images from this time show the tail starting to bend as it adjusts to a change in wind speed and direction.
3. The disconnection occurs while the comet is within the SIR and the tail is carried away with the accelerated plasma. The STEREO images show the tail being completely removed on 2021 December 18 06:08 UTC.

It has to be mentioned that the two solar wind structures (HCS crossing and SIR) are sufficiently close in time that it is not possible to definitively attribute either one as the primary cause due to the expected uncertainty in the model. However, the disconnection event of Leonard seen by STEREO is likely a combination of both these structures, as the event exhibits characteristics of both an HCS crossing and a change in wind speed. It should also be noted that HUXt is one-dimensional and therefore the solar wind direction is always radial. However, from observations of SIRs it is known they produce systematic flow deflections, and it can be assumed that the comet-tail deflection seen is associated with the SIR (Owens & Forsyth 2013).

7. Conclusions

Presented here was an analysis of a comet-tail disconnection event, observed by the STEREO-A HI-2 camera in 2021 December. It was concluded through the comparison of observations from STEREO HI-2 to the output from the solar wind model HUXt, initiated with MAS/BRaVda, that the disconnection event was most likely a result of the comet crossing the HCS and into an SIR.

As well as providing a scientific analysis of a tail disconnection event, more significantly this study also highlights the importance of the use of DA in solar wind models for such studies. Initial analysis of the tail disconnection event prior to DA indicated the HCS crossing to be the only likely candidate for the tail activity, as the model showed no fast solar wind streams within proximity of the comet at the time. This did not support the observations and did not align with previous events and theories. With the addition of DA, the HUXt model confirmed the existence of an SIR, and therefore changed the interpretation of the disconnection event. Furthermore, this research has demonstrated that the HUXt model can be used to reliably examine solar wind interactions for purposes outside its original focus of forecasting Earth-impacting events, and raises the potential of predicting future comet–solar wind interaction events before they occur.

Finally, we would like to note the potential for this study leading to the use of comets as additional in situ measurements for solar wind conditions. As demonstrated, comets can be used to determine the local solar wind speed and indicate the location of the heliospheric current sheet, both of which are important in space-weather forecasting. This information could be fed back into models such as HUXt to improve the output, similar to that achieved in this study using the STEREO-A and ACE data. As well as this, comets provide access to areas of the solar system which are not currently occupied by spacecraft, more specifically higher solar latitudes. Currently, most solar wind models focus on the ecliptic plane as this is where the space weather that affects Earth occurs, but understanding the solar wind at higher latitudes will ultimately lead to an improvement of solar wind models and our understanding of how solar wind structures propagate through the solar system. Comets can be visible in the solar system for months at a time, during which they are often tracked and photographed by amateur astronomers as well as crossing the fields of view of multiple spacecraft. This offers the possibility of a continuous measure of the solar wind conditions at varying solar longitudes and latitudes over time, something that current spacecraft cannot provide.

Events such as these are not only invaluable to the comet community in understanding the mechanisms behind tail disconnections, but also to the solar wind community. Improved observations of solar wind interactions outside of the capabilities of spacecraft enable the possibility of using comets as in situ data points within the harder-to-reach regions of the heliosphere.

Data Availability

The HUXt model used in this research can be downloaded online (https://doi.org/10.5281/zenodo.6794462; Owens & Barnard 2022). HUXt version 4.0 was used in this work. BRaVDA can be accessed from https://doi.org/10.5281/zenodo.7892408 (Lang 2023). The MAS inputs used were obtained from https://www.predsci.com/data/runs/cr2252-high/hmi_mast_mas_std_0101/helio, using the MAS global coronal model to compute the solar wind at 30 $R_\odot$. Heliospheric Imager data were accessed from the UK Solar System Data Centre (http://www.ukssdc.rl.ac.uk/solar/stereo/data.html). The differenced movie of Comet Leonard in STEREO-A HI-2 Camera in 2021 December was downloaded from RAL Space at https://www.stereo.rl.ac.uk/cgi-bin/movies.pl.

ORCID iDs

Sarah R. Watson ⓘ https://orcid.org/0009-0004-6566-6281
Christopher J. Scott ⓘ https://orcid.org/0000-0001-6411-5649
Mathew J. Owens ⓘ https://orcid.org/0000-0003-2061-2453
Luke A. Barnard ⓘ https://orcid.org/0000-0001-9876-4612

References

Alfvén, H. 1942, Natur, 150, 405
Allen, R. C., Ho, G. C., Jian, L. K., et al. 2021, A&A, 650, A25
Antiochos, S. K., Mikić, Z., Titov, V. S., Lionello, R., & Linker, J. A. 2011, ApJ, 731, 112
Arge, C. N., & Pizzo, V. J. 2000, JGRA, 105, 10465
Barnard, L., & Owens, M. 2022, FrP, 10, 1005621

Brandt, J. C., Caputo, F. M., Hoeksema, J. T., et al. 1999, Icar, 137, 69
Brosius, J. W., Holman, G. D., Niedner, M. B., et al. 1987, A&A, 187, 267
Delva, M., Schwingenschuh, K., Niedner, M. B., & Gringauz, K. I. 1991, P&SS, 39, 697
Ebert, R. W., McComas, D. J., Elliott, H. A., Forsyth, R. J., & Gosling, J. T. 2009, JGRA, 114, A01109
Edberg, N. J. T., Eriksson, A. I., Odelstad, E., et al. 2016, JGRA, 121, 949
Eyles, C. J., Harrison, R. A., Davis, C. J., et al. 2009, SoPh, 254, 387
Götz, C., Deca, J., Mandt, K., & Volwerk, M. 2022, arXiv:2211.04887
Howard, R. A., Moses, J. D., Vourlidas, A., et al. 2008, SSRv, 136, 67
Jia, Y. D., Combi, M. R., Hansen, K. C., & Gombosi, T. I. 2007, JGRA, 112, 5223
Jia, Y. D., Russell, C. T., Jian, L. K., et al. 2009, ApJL, 696, L56
Jian, L. K., Luhmann, J. G., Russell, C. T., & Galvin, A. B. 2019, SoPh, 294, 31
Jones, G. H., & Brandt, J. C. 2004, GeoRL, 31, L20805
Jones, G. H., Knight, M. M., Battams, K., et al. 2018, SSRv, 214, 20
Kaiser, M. L., Kucera, T. A., Davila, J. M., et al. 2008, SSRv, 136, 5
Kalnay, E. 2002, Atmospheric Modeling, Data Assimilation and Predictability (Cambridge: Cambridge Univ. Press)
Kuchar, T. A., Buffington, A., Arge, C. N., et al. 2008, JGRA, 113, A04101
Lang, M. 2023, University-of-Reading-Space-Science/BRaVDA: BRaVDA v1.9, Zenodo, doi:10.5281/zenodo.7892408
Lang, M., & Owens, M. J. 2019, SpWea, 17, 59
Lang, M., Witherington, J., Turner, H., Owens, M. J., & Riley, P. 2021, SpWea, 19, e2020SW002698

Lundstedt, H., & Magnusson, P. 1987, A&A, 187, 261
Migliorini, S., & Candy, B. 2019, QJRMS, 145, 867
Niedner, M. B., Jr, & Brandt, J. C. 1978, ApJ, 223, 655
Niedner, M. B., Jr, & Brandt, J. C. 1979, ApJ, 234, 723
Owens, M., & Barnard, L. 2022, University-of-Reading-Space-Science/HUXt: HUXt v4.0, Zenodo, doi:10.5281/zenodo.6794462
Owens, M., Lang, M., Barnard, L., et al. 2020, SoPh, 295, 43
Owens, M. J. 2020, Solar-Wind Structure (Oxford: Oxford Univ. Press)
Owens, M. J., & Forsyth, R. J. 2013, LRSP, 10, 5
Owens, M. J., Lang, M., Riley, P., & Stansby, D. 2019, SoPh, 294, 83
Parker, E. N. 1958, ApJ, 128, 664
Price, O., Jones, G. H., Morrill, J., et al. 2019, Icar, 319, 540
Ramanjooloo, Y., & Jones, G. H. 2022, JGRA, 127, e2021JA029799
Riley, P., Linker, J. A., & Mikić, Z. 2001, JGRA, 106, 15889
Riley, P., & Lionello, R. 2011, SoPh, 270, 575
Thomas, S. R., Owens, M. J., Lockwood, M., & Scott, C. J. 2014, SoPh, 289, 2653
Voelzke, M. R. 2005, EM&P, 97, 399
Voelzke, M. R., & Matsuura, O. T. 2000, A&AS, 146, 1
Vourlidas, A., Davis, C., Eyles, C., et al. 2008, ApJL, 668, L79
Wegmann, R. 2000, A&A, 358, 759
Yeates, A. R., Mackay, D. H., van Ballegooijen, A. A., & Constable, J. A. 2010, JGRA, 115, A09112
Yi, Y., Walker, R. J., Ogino, T., & Brandt, J. C. 1994, JGRA, 101, 27585
Zhang, Q., Ye, Q., Vissapragada, S., Knight, M. M., & Farnham, T. L. 2021, AJ, 162, 194